Direct Measurements of Cosmic Rays with the Calorimetric Electron Telescope on the International Space Station

Y. Akaike[1, 2⋆], O. Adriani[3, 4], K. Asano[5], Y. Asaoka[5], E. Berti[3, 4], G. Bigongiari[6, 7], W.R. Binns[8], M. Bongi[3, 4], P. Brogi[6, 7], A. Bruno[9], J.H. Buckley[8], N. Cannady[10, 11, 12], G. Castellini[13], C. Checchia[6, 7], M.L. Cherry[14], G. Collazuol[15, 16], K. Ebisawa[17], A. W. Ficklin[14], H. Fuke[17], S. Gonzi[3, 4], T.G. Guzik[14], T. Hams[10], K. Hibino[18], M. Ichimura[19], K. Ioka[20], W. Ishizaki[5], M.H. Israel[8], K. Kasahara[21], J. Kataoka[22], R. Kataoka[23], Y. Katayose[24], C. Kato[25], N. Kawanaka[20], Y. Kawakubo[14], K. Kobayashi[1, 2], K. Kohri[26], H.S. Krawczynski[8], J.F. Krizmanic[11], P. Maestro[6, 7], P.S. Marrocchesi[6, 7], A.M. Messineo[27, 7], J.W. Mitchell[11], S. Miyake[28], A.A. Moiseev[29, 11, 12], M. Mori[30], N. Mori[4], H.M. Motz[31], K. Munakata[25], S. Nakahira[17], J. Nishimura[17], G.A. de Nolfo[9], S. Okuno[18], J.F. Ormes[32], S. Ozawa[33], L. Pacini[3, 13, 4], P. Papini[4], B.F. Rauch[8], S.B. Ricciarini[13, 4], K. Sakai[10, 11, 12], T. Sakamoto[34], M. Sasaki[29, 11, 12], Y. Shimizu[18], A. Shiomi[35], P. Spillantini[3], F. Stolzi[6, 7], S. Sugita[34], A. Sulaj[6, 7], M. Takita[5], T. Tamura[18], T. Terasawa[5], S. Torii[1], Y. Tsunesada[36, 37], Y. Uchihori[38], E. Vannuccini[4], J.P. Wefel[14], K. Yamaoka[39], S. Yanagita[40], A. Yoshida[34], K. Yoshida[21] and W. V. Zober[8]
(CALET Collaboration)

1 Waseda Research Institute for Science and Engineering, Waseda University, 17 Kikuicho, Shinjuku, Tokyo 162-0044, Japan
2 JEM Utilization Center, Human Spaceflight Technology Directorate, Japan Aerospace Exploration Agency, 2-1-1 Sengen, Tsukuba, Ibaraki 305-8505, Japan
3 Department of Physics, University of Florence, Via Sansone, 1 - 50019, Sesto Fiorentino, Italy
4 INFN Sezione di Florence, Via Sansone, 1 - 50019, Sesto Fiorentino, Italy
5 Institute for Cosmic Ray Research, The University of Tokyo, 5-1-5 Kashiwa-no-Ha, Kashiwa, Chiba 277-8582, Japan
6 Department of Physical Sciences, Earth and Environment, University of Siena, via Roma 56, 53100 Siena, Italy
7 INFN Sezione di Pisa, Polo Fibonacci, Largo B. Pontecorvo, 3 - 56127 Pisa, Italy
8 Department of Physics and McDonnell Center for the Space Sciences, Washington University, One Brookings Drive, St. Louis, Missouri 63130-4899, USA
9 Heliospheric Physics Laboratory, NASA/GSFC, Greenbelt, Maryland 20771, USA
10 Center for Space Sciences and Technology, University of Maryland, Baltimore County, 1000 Hilltop Circle, Baltimore, Maryland 21250, USA
11 Astroparticle Physics Laboratory, NASA/GSFC, Greenbelt, Maryland 20771, USA
12 Center for Research and Exploration in Space Sciences and Technology, NASA/GSFC, Greenbelt, Maryland 20771, USA
13 Institute of Applied Physics (IFAC), National Research Council (CNR), Via Madonna del Piano, 10, 50019, Sesto Fiorentino, Italy
14 Department of Physics and Astronomy, Louisiana State University, 202 Nicholson Hall, Baton Rouge, Louisiana 70803, USA
15 Department of Physics and Astronomy, University of Padova, Via Marzolo, 8, 35131 Padova, Italy
16 INFN Sezione di Padova, Via Marzolo, 8, 35131 Padova, Italy
17 Institute of Space and Astronautical Science, Japan Aerospace Exploration Agency, 3-1-1 Yoshinodai, Chuo, Sagamihara, Kanagawa 252-5210, Japan
18 Kanagawa University, 3-27-1 Rokkakubashi, Kanagawa, Yokohama, Kanagawa 221-8686, Japan

19 Faculty of Science and Technology, Graduate School of Science and Technology, Hirosaki University, 3, Bunkyo, Hirosaki, Aomori 036-8561, Japan
20 Yukawa Institute for Theoretical Physics, Kyoto University, Kitashirakawa Oiwake-cho, Sakyo-ku, Kyoto, 606-8502, Japan
21 Department of Electronic Information Systems, Shibaura Institute of Technology, 307 Fukasaku, Minuma, Saitama 337-8570, Japan
22 School of Advanced Science and Engineering, Waseda University, 3-4-1 Okubo, Shinjuku, Tokyo 169-8555, Japan
23 National Institute of Polar Research, 10-3, Midori-cho, Tachikawa, Tokyo 190-8518, Japan
24 Faculty of Engineering, Division of Intelligent Systems Engineering, Yokohama National University, 79-5 Tokiwadai, Hodogaya, Yokohama 240-8501, Japan
25 Faculty of Science, Shinshu University, 3-1-1 Asahi, Matsumoto, Nagano 390-8621, Japan
26 Institute of Particle and Nuclear Studies, High Energy Accelerator Research Organization, 1-1 Oho, Tsukuba, Ibaraki, 305-0801, Japan
27 University of Pisa, Polo Fibonacci, Largo B. Pontecorvo, 3 - 56127 Pisa, Italy
28 Department of Electrical and Electronic Systems Engineering, National Institute of Technology (KOSEN), Ibaraki College, 866 Nakane, Hitachinaka, Ibaraki 312-8508, Japan
29 Department of Astronomy, University of Maryland, College Park, Maryland 20742, USA
30 Department of Physical Sciences, College of Science and Engineering, Ritsumeikan University, Shiga 525-8577, Japan
31 Faculty of Science and Engineering, Global Center for Science and Engineering, Waseda University, 3-4-1 Okubo, Shinjuku, Tokyo 169-8555, Japan
32 Department of Physics and Astronomy, University of Denver, Physics Building, Room 211, 2112 East Wesley Avenue, Denver, Colorado 80208-6900, USA
33 Quantum ICT Advanced Development Center, National Institute of Information and Communications Technology, 4-2-1 Nukui-Kitamachi, Koganei, Tokyo 184-8795, Japan
34 College of Science and Engineering, Department of Physics and Mathematics, Aoyama Gakuin University, 5-10-1 Fuchinobe, Chuo, Sagamihara, Kanagawa 252-5258, Japan
35 College of Industrial Technology, Nihon University, 1-2-1 Izumi, Narashino, Chiba 275-8575, Japan
36 Graduate School of Science, Osaka Metropolitan University, Sugimoto, Sumiyoshi, Osaka 558-8585, Japan
37 Nambu Yoichiro Institute for Theoretical and Experimental Physics, Osaka Metropolitan University, Sugimoto, Sumiyoshi, Osaka 558-8585, Japan
38 National Institutes for Quantum and Radiation Science and Technology, 4-9-1 Anagawa, Inage, Chiba 263-8555, Japan
39 Nagoya University, Furo, Chikusa, Nagoya 464-8601, Japan
40 College of Science, Ibaraki University, 2-1-1 Bunkyo, Mito, Ibaraki 310-8512, Japan
* CorrespondingAuthor yakaike@aoni.waseda.jp

February 10, 2023

21st International Symposium on Very High Energy Cosmic Ray Interactions (ISVHECRI 2022)
Online, 23-27 May 2022
doi:10.21468/SciPostPhysProc.?

Abstract

The CALorimetric Electron Telescope, CALET, has been measuring high-energy cosmic rays on the International Space Station since October 13, 2015. The scientific objectives addressed by the mission are to search for possible nearby sources of high-energy electrons and potential signatures of dark matter, and to investigate the details of galactic cosmic-ray acceleration and propagation. The calorimetric instrument, which is 30 radiation lengths or 1.3 proton interaction lengths thick with fine imaging capability, is optimized to measure cosmic-ray electrons by achieving large proton rejection and excellent energy resolution well into the TeV region. In addition, very wide dynamic range of energy measurement and individual charge identification capability enable us to measure proton and nuclei spectra from a few tens GeV to a PeV scale. Nearly 20 million cosmic-ray shower events over 10 GeV per month are triggered and the continuous observation has been kept without any major interruption since the start of operation. Using the data obtained over 6.5 years of operation, we will present a brief summary of the CALET observation including electron spectrum, and proton and nuclei spectra as well as the performance study on orbit with MC simulations.

Contents

1 Introduction

The CALorimetric Electron Telescope (CALET), developed and operated by Japan in collaboration with Italy and the United States, is a high-energy astroparticle physics experiment installed on the International Space Station (ISS) [1]. It was launched on August 19, 2015, by a Japanese carrier H-IIB, delivered to the ISS by the HTV-5 Transfer Vehicle, and installed on the Japanese Experiment Module-Exposed Facility (JEM-EF).

The CALET mission addresses several outstanding questions of high-energy astroparticle physics including the origin of cosmic rays (CR), the possible presence of nearby CR sources, the acceleration and propagation of primary and secondary elements in the galaxy, and the signature of dark matter. The detector of CALET is optimized for high precision measurements of the all-electron (electron plus positron) spectrum in the range from 1 GeV to 20 TeV. Given the excellent energy resolution of CALET for electrons, a detailed study of the spectral shape can reveal the presence of nearby sources of acceleration as well as possible indirect signatures of dark matter. With the capability of identification of the individual cosmic-ray elements, CALET is also carrying out direct measurements of the spectra and relative abundance of cosmic-ray nuclei from proton to nickel in the energy range from a few 10's GeV to a PeV scale. The abundances of trans-iron elements up to $Z = 40$ are studied with a dedicated program of long-term observations.

2 The CALET Instrument

CALET is an all-calorimetric instrument, with a total vertical thickness equivalent to 30 radiation lengths(X_0) or 1.3 proton interaction lengths (λ_I), preceded by a charge identification system. The energy measurement relies on two independent calorimeters: a fine-grained preshower IMaging Calorimeter (IMC), followed by a Total AbSorption Calorimeter (TASC). To identify the individual chemical elements, a CHarge Detector (CHD) is placed at the top of the instrument. A schematic overview of the CALET instrument is presented in Fig. 1 with a simulated 1 TeV electron shower. A TeV electromagnetic shower can be fully contained in the detector thanks to the thick calorimeter, and the capability of shower imaging provides us to precisely identify electrons from hadrons.

The CHD has been designed to measure the charge of incident particles. It is made of a double-layered, segmented, plastic scintillator array. Each layer comprises 14 plastic scintillator paddles, with dimensions 450 mm(L)×32 mm(L)×10 mm(H). The scintillation light generated in each paddle is collected and read out by one photo-multiplier tube (PMT). The CHD and related front-end electronics have been designed to provide particle identification over a large dynamic range for charges from $Z = 1$ to 40. The charge resolution is $0.15e$ for carbon and $0.3e$ for iron.

The IMC measures the initial shower development with a fine granularity by using 1 mm square cross-section scintillating fibers (SciFi) individually read out by Multi-Anode PMT. It consists of 7 layers of tungsten plates each separated by 2 layers of SciFi belts arranged in the X and Y directions and capped by an additional X, Y SciFi layer pair. Each SciFi belt is assembled with 448 fibers. The dimensions of the SciFi layers are 448 mm(L)×448 mm(W). The total thickness of the IMC is equivalent to $3X_0$. The thickness of the tungsten plates is $0.2\ X_0$ for the first 5 layers and $1.0\ X_0$ for the last 2 layers.

The TASC is designed to measure the total energy of the incident particle and discriminate the electromagnetic from hadronic showers. It is composed of 12 layers, each consisting of 16 lead tungstate (PWO) logs, each 326 mm (L)× 19 mm(W)× 20 mm(H). Layers are arranged alternatively in X and Y to provide a 3D reconstruction of the showers. The total thickness of the TASC is $27X_0$ and $1.2\lambda_I$ at normal incidence. Each PWO log of the top layer is read out by a PMT to generate a trigger signal. The other layers are read out by Hybrid packages of silicon Avalanche PhotoDiode (APD) and silicon PhotoDiode (PD). The readout front-end system of each pair of APD/PD sensors is configured with a Charge Sensitive Amplifier (CSA) and a pulse shaping amplifier with dual gain. The readout system provides a dynamic range exceeding 6 orders of magnitude which allows each log to measure signals from 0.5 MIPs (Minimum Ionizing Particles to 10^6 MIPs, which corresponds to the energy deposit by a photon-induced 1 PeV shower.

3 Onboard operations and calibrations

The scientific operation started in October of 2015. Since then, the total observation time of CALET is 2,392 days, and more than 1.57 billion events are observed in high energy (HE) trigger mode as of April 30, 2022. The live-time fraction is over 85% for this period.

Energy calibrations of each channel of CHD, IMC, and TASC are performed with cosmic-ray proton and helium events [2]. With their minimum ionizing particles, raw signals are corrected for light output non-uniformity, gain difference among the channels, position and temperature dependence, as well as temporal gain variations. The four gain ranges of each TASC channel are calibrated with flight data and linked together to provide a seamless response spanning more than six orders of magnitude and allowing observations from MIP to PeV showers. The whole dynamic range of each channel in TASC was calibrated by UV laser irradiation on ground before the flight. The accuracy of the Monte Carlo simulations was tested by a several beam tests at CERN-SPS.

4 Results

4.1 All-electron spectrum

The precise measurement of the high-energy electrons provides a unique probe of nearby cosmic-ray accelerators [3]. In addition, the prominent increase of the positron fraction over 10 GeV established by PAMELA [4] and AMS-02 [5] may require a primary source component for positrons in addition to the generally accepted secondary origin. Candidates for such primary sources of astrophysical and dark matter are discussed. Since these primary sources emit electron-positron pairs, it is expected that the all-electron spectrum would exhibit a spectral feature, near the highest energy range of the primary component.

CALET is optimized for the observation of high-energy electrons with the 30 X_0 thick and well-segmented calorimeter, which provides an excellent energy resolution, 2% above 20 GeV, and less proton contamination. Figure 2 shows the updated result of the electron spectrum in 11 GeV to 4.8 TeV based on 1,815 days of flight data corrected with the high-energy shower trigger, which is 2.3 times larger in statistics than the 2nd published paper [6]. The error bars along the horizontal and vertical axes indicate bin width and statistical errors, respectively. The gray band represents the quadratic sum of statistical and systematic errors. Extensive studies on the systematic uncertainties have been performed.

We noticed that CALET's spectrum is well consistent with AMS-02 [7] below 1 TeV, while they use different detection principles, calorimeter versus magnetic spectrometer, and thus their agreement is important factual evidence. On the other hand, the other group of measurements in space, Fermi-LAT [8] and DAMPE [9], show higher spectra, which might suggest the presence of unknown systematic errors. CALET also has observed flux suppression that is consistent with DAMPE within errors above 1 TeV. In addition, no peak-like structure at 1.4 TeV reported by DAMPE was found in CALET data, irrespective of energy binning.

4.2 Proton spectrum

The proton spectrum by CALET was published in 2019 [10] from 10 GeV to 10 TeV based on the 1,054 days of operations. Thanks to the wide dynamic range to measure the energy, CALET covers the wide energy range and confirmed the spectral hardening around 500 GeV. After that, we updated the proton spectrum with higher statistics for 2,272 days and extended the spectrum to 60 TeV [11] as shown in Fig. 3. The low energy part of the proton spectrum below 1 TeV is consistent with AMS-02 [12] and DAMPE [13]. The high energy part of the spectrum above 1 TeV is systematically lower than that of DAMPE, though the difference is

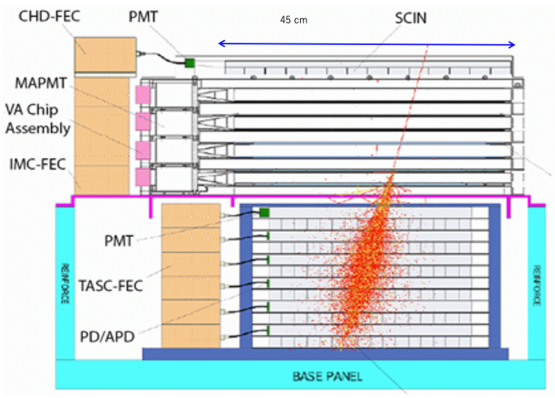

Figure 1: Schematic view of CALET, and 1 TeV simulated electron event is overwritten

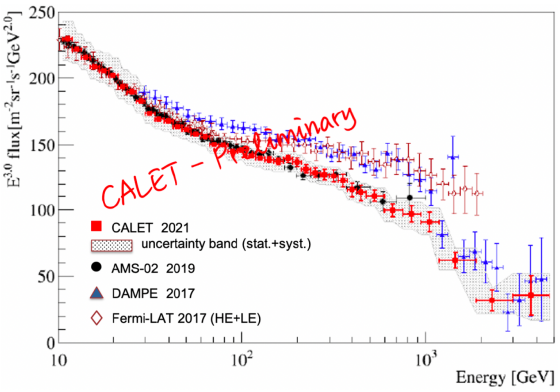

Figure 2: All-electron spectrum measured by CALET, where the gray band indicates the quadrature sum of statistical and systematic errors. Also plotted are direct measurements in space [7–9] for comparison.

within the errors. The spectral hardening break energy observed in CALET is consistent with that of AMS-02 and DAMPE within the errors. Moreover, the spectral softening break energy observed in CALET is consistent with that of DAMPE. These spectral hardening and softening observations contribute to modeling the mechanism of cosmic-ray acceleration and propagation in the Galaxy.

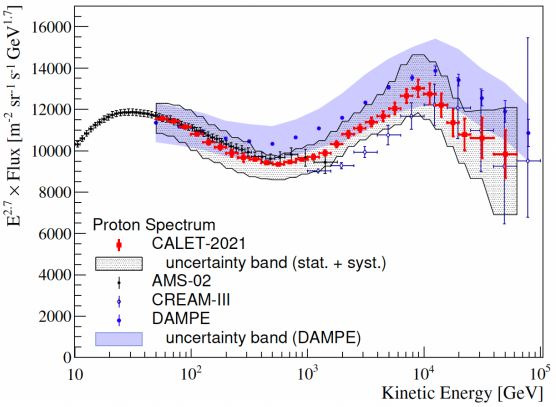

Figure 3: A proton spectrum measured by CALET [11] compared with other results [12–14]. The gray band shows the statistical and systematic uncertainties for CALET.

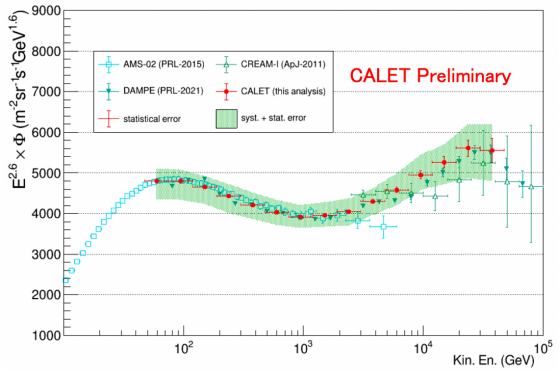

Figure 4: A preliminary helium spectrum measured by CALET compared with other results [15–17]. The gray band shows the statistical and systematic uncertainties for CALET.

4.3 Preliminary helium spectrum

Figure 4 shows the preliminary spectrum of helium with CALET in 1,815 days of operation covering an interval of kinetic energy per particle from 50 GeV to 50 TeV [18], compared with previous observations [15–17]. A progressive hardening up to the multi-TeV region was observed, and the fit in 80 GeV to 20 TeV with a smoothly broken power-low function [16] gives power law index, $\gamma = -2.71 \pm 0.02$, $\Delta\gamma = 0.25 \pm 0.05$ and break energy, $E_0 = 1295 \pm 252$ GeV. These preliminary results are consistent with DAMPE [17] within the errors.

4.4 Carbon and Oxygen Spectra

The energy spectra of carbon and oxygen and their flux ratio measured with CALET based on the 1,480 days of operation in an energy range from 10 GeV/n to 2.2 TeV/n are shown in Fig. 5. The gray band indecates the quadratic sum of statistical and systematic errors [27]. CALET spectra are compared with other direct measurements [19–26]. The carbon spectrum is well consistent with PAMELA and most previous experiments. Both carbon and oxygen spectra between CALET and AMS-02 differ in the absolute normalization, which is lower for CALET by about 27%. They, however, have very similar shapes as indicated by the very consistent measurements of the carbon-to-oxygen ratio. Their spectra can fit with a Double Power-Law (DPL) function:

$$\Phi(E) = \begin{cases} C\left(\frac{E}{\mathrm{GeV}}\right)^{\gamma} & E \le E_0 \\ C\left(\frac{E}{\mathrm{GeV}}\right)^{\gamma}\left(\frac{E}{E_0}\right)^{\Delta\gamma} & E > E_0 \end{cases}$$

where C is the normalization factor, γ the spectral index, and $\Delta\gamma$ the spectral index change above the transition energy E_0. The effect of systematic uncertainties in the measurement of the energy spectrum is modeled in the χ^2 minimization function with a set of 6 nuisance parameters. The DPL fit to the carbon spectrum yields a spectral index $\gamma = -2.663 \pm 0.014$ at energies below the transition region $E_0 = (215 \pm 54)$ GeV/n and a spectral index increase $\Delta\gamma = 0.166 \pm 0.042$ above, with χ^2/d.o.f= 9.0/8. For oxygen, the fit yields $\gamma = -2.637 \pm 0.009$, $E_0 = (264 \pm 53)$ GeV/n, $\Delta\gamma = 0.158 \pm 0.053$, with χ^2/d.o.f= 3.0/8.

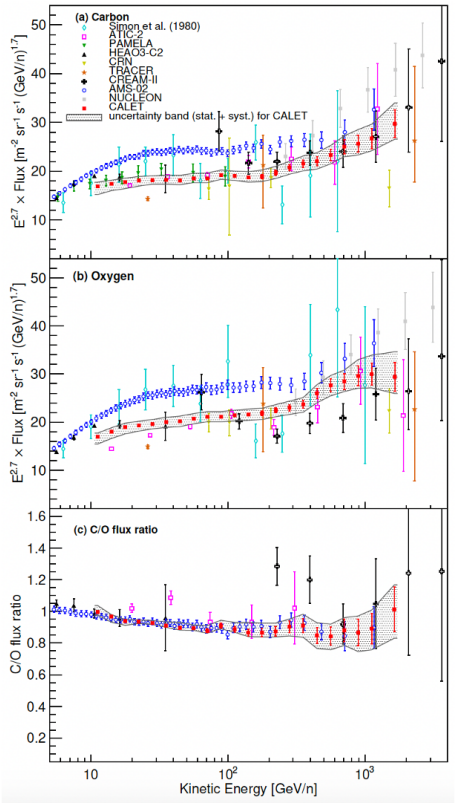

Figure 5: CALET (a) carbon and (b) oxygen spectra multiplied by $E^{-2.7}$ and (c) ratio of carbon to oxygen fluxes. Error bars represent the statistical uncertainty only, the gray band indicates the quadrature sum of statistics and systematic errors. Also plotted are other direct measurements [19–26].

4.5 Iron and Nickel Spectra

Figure 6 shows the iron spectrum in 50 GeV/n to 2.0 TeV/n based on 1,613 days of operations [28]. CALET and AMS-02 [29] iron spectra have a very similar shape and comparable errors, but differ in the absolute normalization of the flux ∼20% like those of carbon and oxygen. Figure 7 shows the nickel spectrum in 8.8 GeV/n to 240 GeV/n [30]. Both CALET iron and nickel spectra are consistent with the hypothesis of a Single Power-Law (SPL) function with a spectral index $\gamma = -2.60 \pm 0.03$ above 50 GeV/n for iron and $\gamma = -2.51 \pm 0.07$ above 20 GeV/n for nickel. The uncertainties given by the present statistics and systematics do not allow us to draw a significant conclusion on a possible deviation from a single power law. The ratio of nickel to iron shows the constant to the energy with 0.061 ± 0.001 within the experimental accuracy. This suggests a similar acceleration and propagation behavior as expected from the less difference in atomic number and weight between Fe and Ni nuclei.

4.6 Preliminary boron spectrum and B/C ratio

Figure 8 shows the preliminary energy spectrum of boron from 16 GeV/n to 2.2 TeV/n [37] compared with PAMELA [25] and AMS-02 [38]. The isotope composition is assumed as

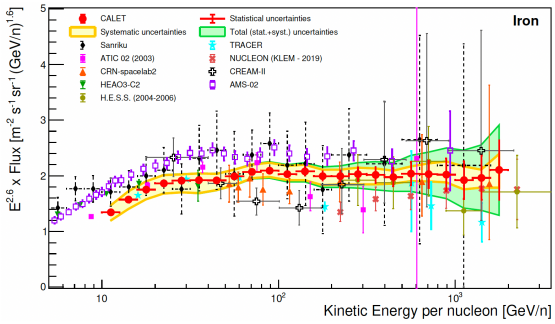

Figure 6: The iron spectrum measured by CALET multiplied by $E^{-2.6}$ as a function of kinetic energy per nucleon. Also plotted are other direct measurements [20–24, 29, 31–33].

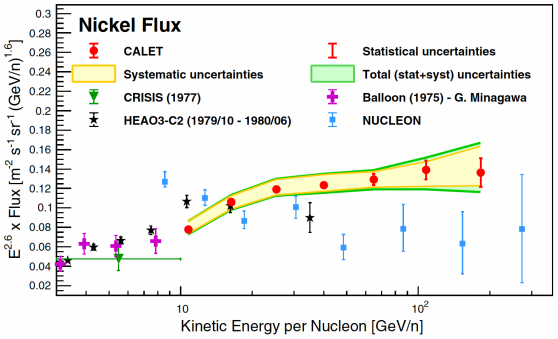

Figure 7: The nickel spectrum measured by CALET multiplied by $E^{-2.6}$ as a function of kinetic energy per nucleon. Also plotted are other direct measurements [20, 34–36].

^{11}B/(^{10}B+^{11}B)= 0.7. CALET boron spectrum is consistent with PAMELA but lower than AMS-02 like the cases of C, O, and Fe spectra. Figure 9 show the preliminary result of B/C ratio from 16 GeV/n to 2.2 TeV/n [37] compared with the previous observations [20, 25, 38–42]. The present result of the B/C ratio can be fitted with a power law function (B/C)= $AE^{-\delta}$, where A is a constant normalization factor, the spectral indices are $\delta = 0.406 \pm 0.039$ in 25 GeV/n withχ^2/ndf= 0.30/3, and $\delta = 0.366 \pm 0.064$ in 100 GeV/n - 2.2 TeV/n withχ^2/ndf= 1.2/7.

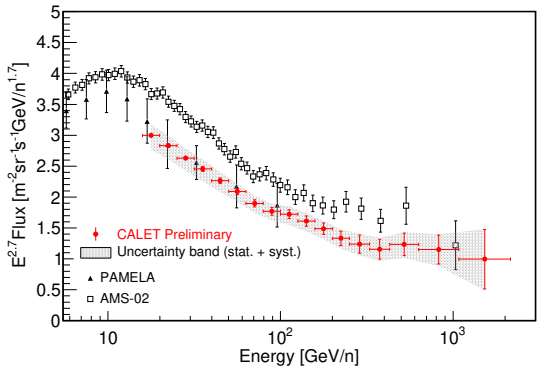

Figure 8: Preliminary energy spectrum of boron as a function of kinetic energy per nucleon with CALET compared with PAMELA [25] and AMS-02 [38].

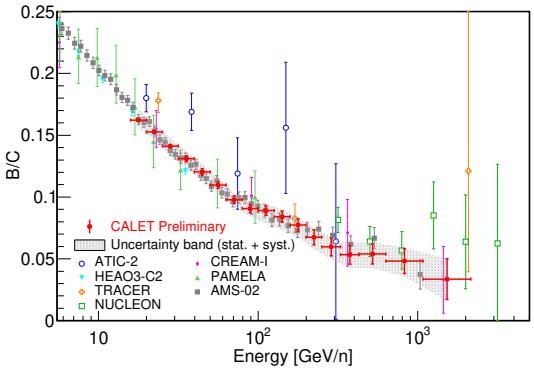

Figure 9: Preliminary result of the boron-to-carbon ratio as a function of kinetic energy with CALET compared with previous observations [20, 25, 38–42].

4.7 Further CALET Observations

In addition to the electrons and nuclei spectra measurements, CALET has been measuring ultra-heavy cosmic-rays (UHCR) with charges $30 \leqq Z \leqq 40$, which are $\sim 10^5$ less abundant than iron. About five years of UHCR observations by CALET collected a data set comparable to that so far collected by the balloon-borne SuperTIGER instrument. Preliminary results of the relative abundances of UHCRs to iron presented at the conference [43] are in reasonable agreement.

CALET observation of low-energy CRs has been successfully performed with a Low-Energy Electron (LEE) shower trigger mode activated at the high geomagnetic latitude [44]. The

count rates of electrons and protons measured by CALET during the solar minimum have reached their maximum, which is comparable to or exceeding the maximum flux observed with PAMELA in the previous solar minimum period. It was also found the modulation amplitude of electron count rate is clearly larger than that of proton count rate, being consistent with the expected charge sign dependence of solar modulation [44].

Moreover, CALET is sensitive to gamma rays from 1 GeV to 10 TeV [45, 46]. Transient events such as gamma-ray bursts in the hard X-ray and soft gamma-ray band have been observed by the CALET gamma-ray burst monitor and the calorimeter. The follow-up campaign for the search for electromagnetic counterparts of the gravitational wave events has been also participated [47].

5 Summary

CALET instrument performance on the ISS has been very stable since the start of the operation on October 13, 2015. Careful calibrations using non-interacting protons and helium events have been successfully carried out, and the linearity of the energy measurements up to 10^6 MIPs was established based on observed events.

At this conference, CALET presented various results including the electron and positron spectrum up to 4.8 TeV [48], a preliminary update of the proton spectrum to 60 TeV [49], and a preliminary helium spectrum to 50 TeV [18]. The spectra of carbon and oxygen and their ratio to 2.2 TeV/n were published in [27]. The iron spectrum to 2.0 TeV/n and nickel spectrum to 240 GeV/n were also published in [28, 30]. Preliminary results of the boron spectrum and the B/C ratio were also presented [37]. In addition, CALET has the potential to study the UHCR, as well as gamma-ray measurements, GRB observations, searches of GW event counterparts, DM searches, and space weather observations.

CALET observation has been carried out over six years and was approved to be extended until the end of 2024 (at least). Improved statistics and refinement of the analysis with additional data will allow to extend the measurements at higher energies and improve the spectral analysis, which will contribute to a further understanding of cosmic rays.

Acknowledgements

We gratefully acknowledge JAXA's contributions to the development of CALET and to the operations onboard the ISS. We also express our sincere gratitude of ASI and NASA for their support of the CALET project. This work was supported in part by JSPS KAKENHI Grants No. 26220708, No. 19H05608 and No. 21K03592 and by the MEXT-Supported Program for the Strategic Research Foundation at Private Universities (2011-2015) (No. S1101021) at Waseda University. The CALET effort in Italy in supported by ASI under Agreement No. 2013-018-R.0 and its amendments. The CALET effort in the U.S. is supported by NASA through Grants No. 80NSSC20K0397, No 80NSSC20K0399, and No. NNH18ZDA001N-APRA18-004.

References

[1] P. S. Marrocchesi *et al.*, PoS(ICRC2021) 010 (2021).

[2] Y. Asaoka, Y. Akaike, Y. Komiya *et al.*, Astropart. Phys. **91**, 1 (2017).

[3] T. Kobayashi, Y. Komori, K. Yoshida *et al.*, Astrophys. J. **601**(1), 340 (2004).

[4] P. Picozza, O. Adriani, G. C. Barbarino *et al.*, Nature (London) **458**(7238), 607 (2009).

[5] M. Aguilar, G. Alberti, B. Alpat *et al.*, Phys. Rev. Lett. **110**, 141102 (2013).

[6] O. Adriani, Y. Akaike, K. Asano *et al.*, Phys. Rev. Lett. **120**, 261102 (2018).

[7] M. Aguilar, D. Aisa, B. Alpat *et al.*, Phys. Rev. Lett. **113**, 221102 (2014).

[8] S. Abdollahi, M. Ackermann, M. Ajello *et al.*, Phys. Rev. D **95**, 082007 (2017).

[9] Q. An, R. Asfandiyarov, P. Bernardini *et al.*, Nature (London) **552**(7683), 63 (2017).

[10] O. Adriani, Y. Akaike, K. Asano *et al.*, Phys. Rev. Lett. **122**, 181102 (2019).

[11] O. Adriani, Y. Akaike, K. Asano *et al.*, Phys. Rev. Lett. **129**, 101102 (2022).

[12] M. Aguilar, D. Aisa, B. Alpat *et al.*, Phys. Rev. Lett. **114**, 171103 (2015).

[13] R. Asfandiyarov, M. S. Cai, J. Chang *et al.*, Science adv. **5**(9), eaax3793 (2019).

[14] Y. S. Yoon, T. Anderson, A. Barrau *et al.*, Astrophys. J. **839**(1), 5 (2017).

[15] Y. S. Yoon, H. S. Ahn, P. S. Allison *et al.*, Astrophys. J. **728**(2), 122 (2011).

[16] M. Aguilar, D. Aisa, B. Alpat *et al.*, Phys. Rev. Lett. **115**, 211101 (2015).

[17] F. Alemanno, Q. An, P. Azzarello *et al.*, Phys. Rev. Lett. **126**, 201102 (2021).

[18] P. Brogi, K. Kobayashi *et al.*, PoS(ICRC2021) 101 (2021).

[19] M. Simon, H. Spiegelhauer, W. K. H. Schmidt *et al.*, Astrophys. J. **239**, 712 (1980).

[20] J. J. Engelmann, P. Ferrando, I. L. Rasmussen *et al.*, Atron. Astrophys. **233**(1), 96 (1990).

[21] D. Müller, S. P. Swordy, P. Meyer *et al.*, Astrophys. J. **374**(1), 356 (1991).

[22] M. Ave, P. J. Boyle, F. Gahbauer *et al.*, Astrophys. J. **678**(1), 262 (2008).

[23] H. S. Ahn, P. Allison, M. G. Bagliesi *et al.*, Astrophys. J. **707**(1), 593 (2009).

[24] A. D. Panov, J. H. Adams, H. S. Ahn *et al.*, Bull. Russ. Acad. Sci. **73**(5), 564 (2009).

[25] O. Adriani, G. C. Barbarino, G. A. Bazilevskaya *et al.*, Astrophys. J. **791**(2), 93 (2014).

[26] E. Atkin, V. Bulatov, V. Dorokhov *et al.*, J. Cosmo. Astropart. Phys. **2017**(7), 20 (2017).

[27] O. Adriani, Y. Akaike, K. Asano *et al.*, Phys. Rev. Lett. **125**, 251102 (2020).

[28] O. Adriani, Y. Akaike, K. Asano *et al.*, Phys. Rev. Lett. **126**, 241101 (2021).

[29] M. Aguilar, L. A. Cavasonza, M. S. Allen *et al.*, Phys. Rev. Lett. **126**, 041104 (2021).

[30] O. Adriani, Y. Akaike, K. Asano *et al.*, Phys. Rev. Lett. **128**, 131103 (2022).

[31] V. Grebenyuk, D. Karmanov, I. Kovalev *et al.*, Adv. Space Res. **64**(12), 2546 (2019).

[32] M. Ichimura, M. Kogawa, S. Kuramata *et al.*, Phys. Rev. D **48**, 1949 (1993).

[33] F. Aharonian, A. G. Akhperjanian, A. R. Bazer-Bachi *et al.*, Phys. Rev. D **75**, 042004 (2007).

[34] M. Minagawa, Astrophys. J. **248**, 847 (1981).

[35] J. S. Young, P. Freier, C. Waddington *et al.*, Astrophys. J. **246**, 1014 (1981).

[36] V. Grebenyuk, D. Karmanov, I. Kovalev *et al.*, arXiv: 1809.07285 (2018).

[37] Y. Akaike, P. Maestro *et al.*, PoS(ICRC2021) 112 (2021).

[38] M. Aguilar, L. Ali Cavasonza, G. Ambrosi *et al.*, Phys. Rev. Lett. **120**, 021101 (2018).

[39] A. Panov, N. Sokolskaya, J. Adams Jr. *et al.*, arXiv: 0707.4415 (2007).

[40] H. Ahn, P. Allison, M. Bagliesi *et al.*, Astropart. Phys. **30**(3), 133 (2008).

[41] A. Obermeier, P. Boyle, J. Hörandel *et al.*, Astrophys. J. **752**(1), 69 (2012).

[42] V. Grebenyuk, D. Karmanov, I. Kovalev *et al.*, Adv. Space Res. **64**(12), 2559 (2019).

[43] W. V. Zober, B. F. Rauch, A. Flcklin *et al.*, PoS(ICRC2021) 124 (2021).

[44] S. Miyake *et al.*, PoS(ICRC2021) 1270 (2021).

[45] N. Cannady *et al.*, PoS(ICRC2021) 604 (2021).

[46] M. Mori *et al.*, PoS(ICRC2021) 619 (2021).

[47] O. Adriani, Y. Akaike, K. Asano *et al.*, Astrophys. J. **933**(1), 85 (2022).

[48] S. Torii, Y. Akaike *et al.*, PoS(ICRC2021) 105 (2021).

[49] K. Kobayashi, P. S. Marrocchesi *et al.*, PoS(ICRC2021) 098 (2021).